# Parametric Investigations of Blade-Vortex Interaction using Large-Eddy Simulation

Marcel Ilie, Fred Nitzsche, Edgar Matida
Department of Mechanical and Aerospace Engineering, Carleton University
Ottawa, Canada
milie@connect.carleton.ca

**The influence of blade-vortex vertical miss-distance and angle of attack on the helicopter blade-vortex mechanism of interaction is investigated using large-eddy simulation (LES). A large-eddy simulation is carried out for a quasi 3-D blade-vortex interaction (BVI) problem, for a subsonic flow M = 0.3 and a chord based Reynolds number of $1.3 \times 10^6$. Computations are carried out to investigate the influence of angle of attack ($\alpha = 0^0$, $\alpha = 5^0$, $\alpha = 10^0$) on the aerodynamic coefficients and acoustic field. It was observed that the blade-vortex vertical miss distance and angle of attack has significant influence on the aerodynamic coefficients and acoustic field.**

## Introduction

In rotorcraft, blade-vortex interaction is one of the main sources of noise and vibrations, and comprises one of the most complex unsteady flow features of helicopter rotor in forward flight. Strong interactions which result in strong chordwise temporal pressure variations are caused by a vortex whose axis is parallel (or nearly parallel) to the spanwise axis of the blade.

BVI noise occurs mainly during landing-descending flight, and sometimes in manoeuvring flight, when the rotating blades pass in close proximity to the previously shed rotor tip vortices. These vortices induce sharp periodic aerodynamic disturbances on the blades, which generate highly impulsive BVI noise. The radiated noise is dependent on the blade-vortex vertical miss distance and the characteristics of previously shed vortex (vortex core size and vortex strength). BVI is most prominent during slow-speed descent, since during this phase of the flight the vortex is more likely to interact with the rotor blades. BVI noise is radiated generally downward and usually dominates other noise sources when it occurs; during most landing descent approach conditions.[1] When a vortex is shed from the rotating blade tip and convected downstream, it is intersected by the next rotor blade. At the start of the BVI, the vortex is at an upstream location and is moving toward the airfoil leading edge, as schematically presented in Figure 1.

Previous studies have indicated that the unsteady lift depends on the vortex strength, vortex core size and blade-vortex vertical miss distance.[2-5] In the present analysis, the influence of vortex core size on the aerodynamic coefficients and aeroacoustic field is subject of investigation. For the past years, the BVI phenomenon has been investigated both experimentally and numerically.[1-13]

Numerical simulation of BVI has been of interest to Computational Fluid Dynamics (CFD) for many years.[5-13] There are still difficulties concerning an accurate numerical prediction of BVI. One of the main issues is the inherent numerical dissipation of CFD models, which severely affects the preserving of the vortex characteristics.

Accurate prediction of BVI aerodynamic loads and aeroacoustics using URANS is known to be very challenging due to the complex unsteady flow dynamics, involving boundary layer development on the suction side and flow separation.[7-10] The use of RANS methods, significantly rely on turbulence models to capture all the relevant turbulence scales. RANS methods predict the noise using the mean flow properties. Due to the fact that noise generation is a multi-scale problem, involving a wide range of length and time scales, the use of RANS-based prediction methods remains limited. Although RANS methods are useful for predicting the aerodynamic coefficients, holding accurately up to some extent, they are usually not suitable or reliable for an accurate noise prediction.

The recent improvements in the processing speed of computers make the applicability of Direct Numerical Simulation (DNS) and Large Eddy Simulation (LES) to turbulent flows more feasible. However, due to a wide range of length and time scales present in turbulent flows, the use of DNS is still limited to low-Reynolds-number flows and relatively simple geometries. It is known that the

number of grid points required for DNS is proportional to $Re^{9/4}$. Direct Numerical Simulation of high-Reynolds number flows of practical interest would necessitate high resolution grid requirements that are far beyond the capability of the most powerful computers available now days. In order to overcome the grid requirements issues, turbulence has to be modelled in order to perform simulations for problems of practical interest. Large-eddy simulation, with a lower computational cost, is a promising alternative method to DNS, for simulations of high Reynolds-number flows. LES methods are capable of simulating flows at high Reynolds number, LES method being independent of Reynolds number. In Large Eddy Simulation, the large scales are directly solved, while the small scales are modelled. Since noise generation is an unsteady process, LES is probably the most affordable computational tool to be used, since it is the only way, other than DNS, to obtain a time-accurate unsteady solution.

**Computational method and models**

The 2-D simulations were performed for Re = $1.3 \times 10^6$, based on free stream velocity $U_\infty$ and the chord length of the airfoil. An airfoil with the chord c = 0.2m is centered in the computational domain whose outer boundary is a square with the side equal to 9c and a spanwise size of 0.1c. The computational domain consists of 2.6 millions grid points with a cluster of grid points around the airfoil and a grid expansion factor of 0.1. For all the computations in this present analysis, a dimensionless time step $\overline{\Delta t} = \Delta t U_\infty / c = 1 \times 10^{-6}$ is chosen, where $U_\infty$ is the free- stream velocity. The time-step is determined with respect to the explicit time-marching scheme and temporal resolution requirement of LES (CFL $\leq$ 1). The flow field is solved using the filtered Navier-Stokes equations along with a standard subgrid scale model and van Driest wall damping.

The core size of the vortex is equal to c/4, where c is the chord of the airfoil and the strength of the vortex is 25% higher than the uniform free-stream velocity. Three different test cases are investigated based on the vortex-airfoil vertical miss-distance, h = 0.00 m, h = - 0.01m and h = - 0.02m.

A schematic view of the test case, $\alpha = 0^0$ is presented in Figure 1.

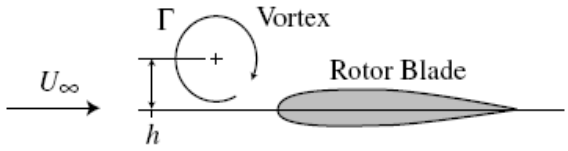


Figure 1. Schematic view of blade-vortex interaction

For all test cases, the releasing location of the vortex is $x_v$ = 0.13m upstream of the leading edge. No slip boundary conditions are used at the airfoil wall. Free slip boundary conditions are used at the top and bottom walls with opening at the end of the computational domain.
Parallel processing is invoked in the present analysis and a cluster of computers having 32 CPUs, 2GB memory per processor is used in the simulations.

**Results and Discussion**

Figure 2 presents the LES results of instantaneous magnitude of velocities for an angle of attack $\alpha = 0^0$, at five different instants in time as a clockwise rotating vortex travels at three different vertical miss-distances, h = 0.00 m.

Independent of vortex-airfoil vertical miss distance, the airfoil sees an induced velocity from the vortex, pointed downward. From Figure 2, it is apparent that the vortex core is almost destroyed as the vortex interacts directly with the airfoil (h = 0.00 m), and there are wake perturbations due to the presence of the remaining vortex in the flow field. Also it can be seen that as the vortex approaches the airfoil and travels the chord length of airfoil, the velocity distribution on the upper and lower surface of the airfoil changes continuously until the vortex leaves the airfoil. However increasing the vortex-airfoil vertical miss distance, the lower surface of the airfoil sees a higher velocity as the vortex encounters the airfoil.

The change in velocity distribution field influences the pressure distribution around the airfoil and causes fluctuations of the stagnation point along the upper and lower surface of the airfoil. When the vortex is in the length of one chord downstream the airfoil, Figure 2a, t = 0.0044 s, the wake is disturbed by the presence of the residual component of the vortex. As the residual component of the vortex travels far downstream, it merges into the airfoil wake and there is a significant mixing with the airfoil wake, causing a fast dissipation of the residual component of vortex.

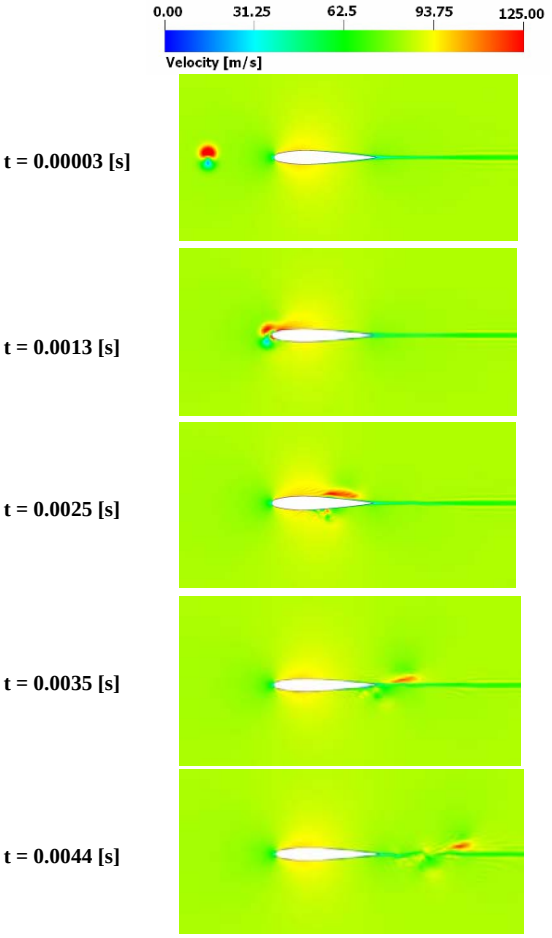


h = 0.00 m

Figure 2. Time evolved fluid structures (velocity magnitude), angle of attack $\alpha = 0^o$

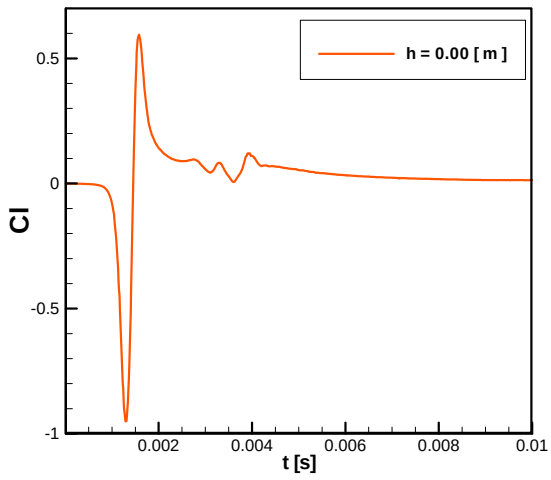


Figure 3. Time history of lift coefficient, $\alpha = 0^o$

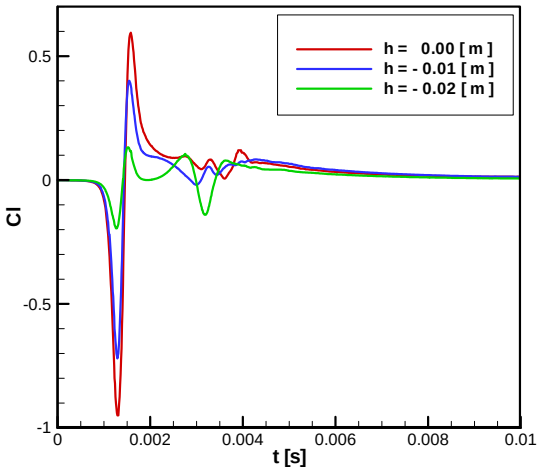


Figure 4. Comparison of lift coefficient, $\alpha = 0^o$

The influence of vortex-airfoil mechanism of interaction is reflected into the aerodynamic coefficients and this can be seen from Figure 3 and Figure 5.

Figure 3 shows the temporal variation of lift coefficient for the case of a vortex superimposed on a uniform flow encountering a NACA 0012 airfoil at a zero angle of attack and a vertical miss-distance h = 0.00 m. The lift coefficient is influenced by the pressure distribution over the airfoil surface. From Figure 3, it can be seen that there is a continuous decrease in lift as the vortex approaches the airfoil (until a minimum value of lift is achieved), followed by a sudden jump as the vortex core passes the airfoil leading edge. This sudden jump in lift coefficient is generated by a sudden change in the pressure coefficient. The sudden change in pressure coefficient has an aeroacoustic meaning and is associated with Blade-Vortex Interaction (BVI) aeroacoustic noise, when the vortex encounters the airfoil. Although there is an increase of lift coefficient value when the vortex passes the leading edge, the absolute value of this maximum is smaller than the absolute minimum value described above. This difference in minimum-maximum absolute values is due to the vortex core distortion when the vortex encounters the airfoil. When the residual component of the distorted vortex is far downstream from the airfoil, the lift coefficient converges asymptotically to a zero value and the flow field is almost undisturbed. An important result is the fact that when the vortex-airfoil vertical miss distance is zero, although the amplitudes of lift coefficient are high, the fluctuations of lift coefficient when the vortex travels the chord length of airfoil are small and this is a result of the vortex core distortion as well. Also for a vertical miss distance h = 0.00m, there are fluctuations in lift coefficient as the residual component of the distorted vortex leaves the

airfoil and merges into the airfoil wake, at the instant t = 0.0035s.

Similar behavior of the lift coefficient was observed for the other two test cases h = - 0.01m and h = - 0.02m and therefore a comparison of time varying lift coefficient for all three test cases would be more appropriate rather than a detailed description of each test case alone.

In this sense, Figure 4 presents a comparison of the lift coefficient for three different vortex-airfoil vertical miss distances h = 0.00m, h = - 0.01m and h = - 0.02m. For all test cases, lift coefficient presents a sudden jump at the instant when the vortex encounters the airfoil (t = 0.0013s). The amplitude of the lift jump decreases as the vortex-airfoil vertical miss distance increases. This decrease is due to the fact that the vortex-airfoil interactions are less significant and have less impact on the flow field. From the comparison of lift coefficient, it can be seen that with the increase of vortex-airfoil vertical miss distance, the jump in lift coefficient at t = 0.0013s tends to become more symmetric with respect to a zero value and the transition from negative to positive values is smoother.

Large fluctuations in lift coefficient can be observed when the vortex travels the airfoil chord length for a vertical miss-distance h = - 0.02m. This is a consequence of the fact that the vortex-airfoil interactions are less and less severe; the vortex preserves better its characteristics (core size and strength) and has a more significant influence on the flow field. While the vortex travels away from the airfoil, the lift coefficient converges to zero from positive values for all cases.

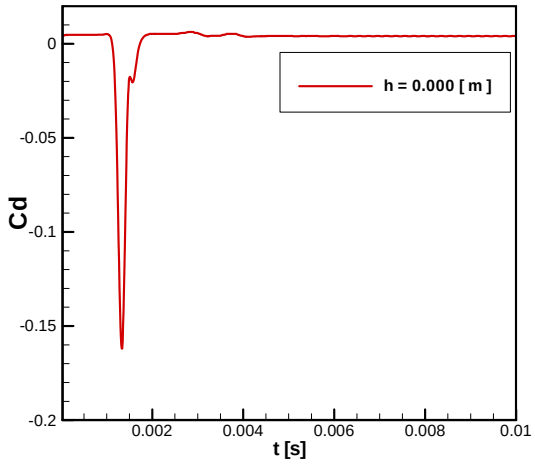


Figure 5. Time history of drag coefficient, $\alpha = 0^o$

Similar to the lift coefficient, the presence of the vortex in the flow field influences the drag coefficient as well. For the case of a uniform flow past a NACA 0012 airfoil, at angle of attack $\alpha = 0^o$, the drag coefficient is constant and has the value of $C_d = 0.006$, for a Reynolds number $1.3x10^6$.

Figure 5 presents the time varying drag coefficient for the case of a vortex superimposed on a uniform flow encountering a NACA 0012 airfoil at a zero angle of attack and a vertical miss-distance h = 0.00 m. At the instant when the vortex encounters the airfoil (t = 0.0013s), separation occurs. As a result of the vortex-airfoil mechanism of interaction, reverse flow is generated, and this is indicated by the negative values of drag coefficient. The vortex–airfoil mechanism of interaction has a significant impact on the drag coefficient, reflected by the large negative value of drag coefficient, $C_d = - 0.163$. Oscillations of drag coefficient are observed as the vortex travels the first half of the chord length of the airfoil, at the instant t = 0.0016s. As the residual component of the vortex travels downstream the airfoil, the drag coefficient reaches a constant value of $C_d = 0.006$, which corresponds to the case of uniform flow past a NACA 0012 airfoil, at angle of attack $\alpha = 0^o$

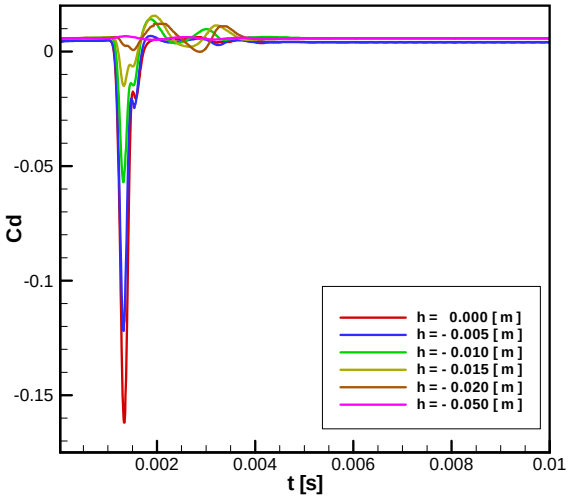


Figure 6. Comparison of drag coefficient, $\alpha = 0^o$

Figure 6 presents the comparison of time varying drag coefficient for six different test cases, based on the vortex–airfoil vertical miss distance h. For most of test cases, large negative values of drag coefficient are observed at the instant when the vortex encounters the airfoil, t = 0.0013 s. These negative values are caused primarily by separation and reverse flow over the surface of the airfoil. It can be

seen that the largest amount of reverse flow occurs when the vortex–airfoil vertical miss distance h is small. For the case of vertical miss distance, h = 0.000m, the vortex encounters the airfoil frontally and the interaction is very strong, causing a severe distortion of the vortex. As the vortex–airfoil vertical miss distance increases, the interactions are less and less severe and likewise the separation, resulting in a decrease of magnitude of the negative peaks of drag coefficient associated with reverse flow. From Figure 6 it can be seen that a small change in the vortex–airfoil vertical miss distance has a large impact on the drag coefficient at the instant when the vortex encounters the airfoil, t = 0.0013s. Due to the vortex-airfoil mechanism of interaction, the distorted vortex causes fluctuations of drag coefficient as it travels the chord length of airfoil. From the drag coefficient comparison, Figure 6, it can be seen that with the increase of vortex-airfoil vertical miss distance, as the vortex travels the chord length of the airfoil, the fluctuations of drag coefficient increase. This is a consequence of the influence of vortex-airfoil vertical miss distance, h, on the mechanism of interaction. Increasing the vortex-airfoil vertical miss distance, the interactions become less and less severe; the vortex preserving better its characteristics and have a more significant impact on the flow field, disturbing it. The disturbances of the flow field are reflected into the fluctuations of the aerodynamic coefficients. As the residual component of the vortex leaves the airfoil, the drag coefficient reaches a constant value $C_d$ = 0.006; value which corresponds to the case of a uniform flow past a NACA 0012 airfoil at angle of attack $\alpha$ = 0°, for a Reynolds number 1.3 x $10^6$.

Figure 7 shows the LES results of instantaneous magnitude of velocities for an angle of attack $\alpha$ = 5°, at five different instants in time as a clockwise rotating vortex travels at three different vertical miss-distances, h = 0.00 m. Similar to test case $\alpha$ = 0°, for an angle of attack $\alpha$ = 5°, the airfoil also sees an induced velocity from the vortex, pointed downward. The vortex-airfoil mechanism of interaction for a vertical miss distance h = 0.00 m is associated with distortion of the vortex and an increase of velocity, as well large flow separation at the upper surface of airfoil as seen in Figure 7a. However, there is a significant amount of the remaining vortex traveling downstream and interacting with the airfoil wake and disturbing it.

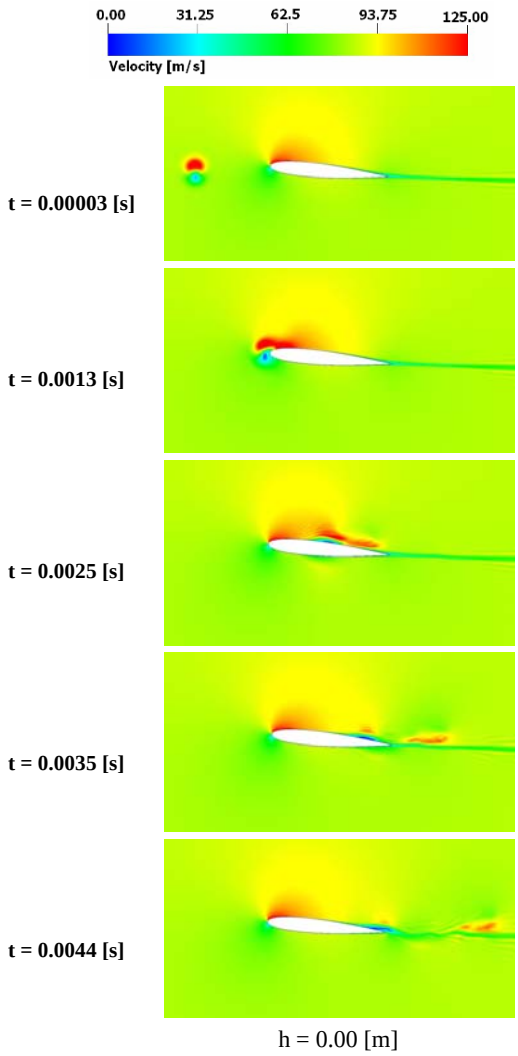


Figure 7. Time evolved fluid structures (velocity magnitude), angle of attack $\alpha$ = 5°

The disturbance of the flow field by the presence of the vortex and the vortex-airfoil mechanism of interaction is reflected into the time variation of the aerodynamic coefficients as presented in Figure 8 and Figure 9. The vortex-airfoil mechanism of interaction is a function of both, airfoil angle of attack and vortex-airfoil vertical miss distance. The lift coefficient exhibits similar behavior for the two angles of attack, $\alpha$ = 0° and $\alpha$ = 5°, at the instant when the vortex encounters the airfoil (t = 0.0013s). From Figure 8, it can be seen that there is a continuous decrease in lift as the vortex approaches the airfoil, followed by a sudden jump as the vortex core passes the airfoil leading edge. Due to the vortex-airfoil mechanism of interaction, small scale vortices are generated causing significantly large fluctuations of lift coefficient at the instant when the

vortex leaves the airfoil, Figure 8, at the instant t = 0.0035s.

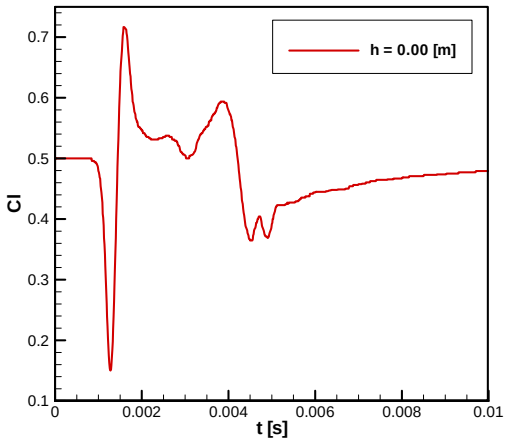


Figure 8. Time history of lift coefficient, $\alpha = 5^o$

Figure 9 presents the influence of vortex-airfoil vertical miss distance on the mechanism of interaction, for a constant angle of attack $\alpha = 5^o$. It can be seen that for all test cases, the lift coefficient presents similar behavior at the instant when the vortex encounters the airfoil, t = 0.0013s. The influence of vortex-airfoil vertical miss distance on the mechanism of interaction is reflected in the scale of the lift coefficient amplitudes. From Figure 9, it can be seen that independent of the vertical miss distance value, the lift coefficient follows almost the same pattern up to the instant when the vortex leaves the airfoil, t = 0.0035s. However, the influence of the vertical miss distance on the mechanism of interaction can be observed after the instant when the vortex leaves the airfoil. Hence, large differences in lift coefficient values can be seen as the residual component of the distorted vortex leaves the airfoil and travels downstream. It is worth to notice that for the test cases h = - 0.01m, h = - 0.015m and h = - 0.02m, the lift coefficient exhibits very similar trend as the residual component of the distorted vortex leaves the airfoil and travels downstream. The fluctuations of lift coefficient (while the vortex travels the chord length of the airfoil) are more significant as the vertical miss distance increases. This is a result of the vortex-airfoil mechanism of interaction. Increasing the vortex-airfoil vertical miss distance, the interactions are less severe and the vortex is less distorted, preserving better its characteristics. As a consequence, the vortex has a stronger impact on the near flow field, disturbing it significantly. However, the amplitudes of lift coefficient fluctuations decrease with the increase of the vertical miss distance.

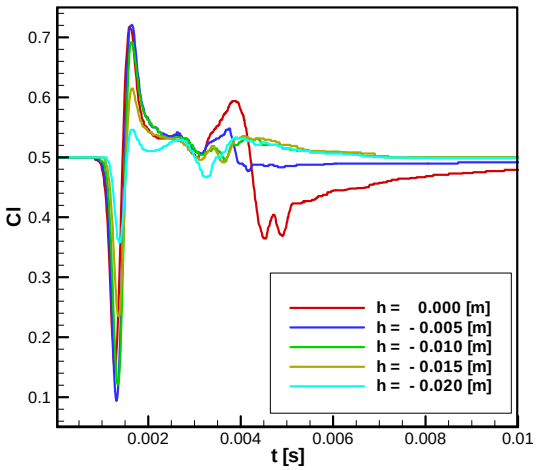


Figure 9. Comparison of lift coefficient, $\alpha = 5^o$

Figure 10 presents the time varying drag coefficient for the case of angle of attack $\alpha = 5^o$ and vortex-airfoil vertical miss distance h = 0.00m. For the case of uniform flow past a NACA 0012 airfoil, at angle of attack $\alpha = 5^o$, the drag coefficient is constant and has the value of $C_d$ = 0.0073, for a Reynolds number 1.3 x $10^6$.

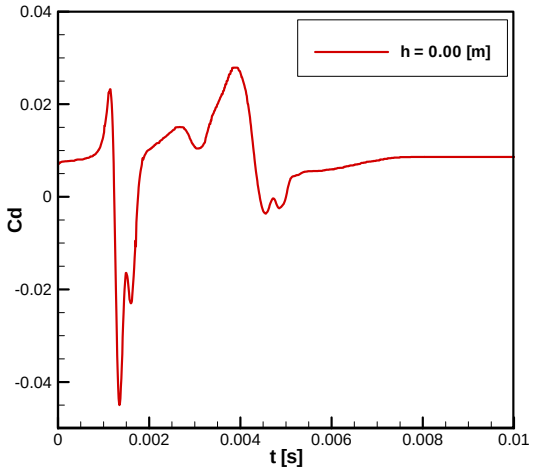


Figure 10. Time history of drag coefficient, $\alpha = 5^o$

From Figure 10, it can be seen that there is a continuous increase of drag coefficient as the vortex approaches the

airfoil, followed by a sudden decrease as the vortex core passes the airfoil leading edge. Similar to the case of angle of attack $\alpha = 0^o$, the flow separation is also observed for the case of angle of attack $\alpha = 5^o$, at the instant when the vortex encounters the airfoil, t = 0.0013s. Also reverse flow is generated, and this is indicated by the negative values of drag coefficient, $C_d$ = - 0.045. Large fluctuations of drag coefficient can be seen at the instant when the residual component of the vortex leaves the airfoil, t = 0.0035s. Also reverse flow is generated at the instant when the vortex leaves the airfoil, indicated by negative values of drag coefficient, $C_d$ = - 0.005, at the instant t = 0.0045s. The presence of reverse flow at the instant when the vortex leaves the airfoil is a result of the influence of angle of attack on the vortex-airfoil mechanism of interaction. Also oscillations of drag coefficient are observed as the vortex travels the chord length of the airfoil. As the residual component of the vortex travels downstream the airfoil, the drag coefficient converges to a constant value of $C_d$ = 0.0073; corresponding to the case of uniform flow past NACA0012 at angle of attack $\alpha = 5^o$.

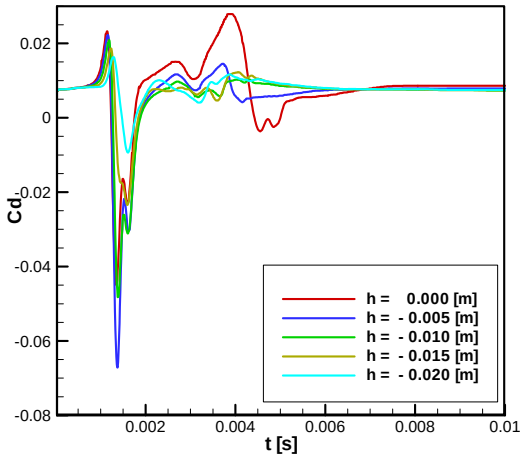


Figure 11. Comparison of drag coefficient, $\alpha = 5^o$

Figure 11 presents the comparison of time varying drag coefficient for an angle of attack $\alpha = 5^o$, for five different test cases, based on the vortex–airfoil vertical miss distance h. For most of test cases, large negative values of drag coefficient are observed at the instant when the vortex encounters the airfoil, t = 0.0013s. These negative values are caused primarily by separation and reverse flow over the surface of the airfoil. Similar to the test case of an angle of attack $\alpha = 0^o$, for an angle of attack $\alpha = 5^o$ it also can be seen that the largest amount of reverse flow occurs when the vortex–airfoil vertical miss distance h is small. However, it is important to notice that besides these similarities, there are still significant differences between the two test cases corresponding to angles of attack $\alpha = 0^o$ and $\alpha = 5^o$ when comparing the values of drag coefficient, for different vortex-airfoil vertical miss distances. Hence, for an angle of attack $\alpha = 5^o$, the drag coefficient exhibits the largest negative value, associated with the reverse flow, for a vertical miss distance h = - 0.005m. For the case of angle of attack $\alpha = 5^o$, there is not a direct relationship of drag coefficient function of vertical miss distance as it was observed for the case of an angle of attack $\alpha = 0^o$. This fact is associated with the influence of angle of attack on the vortex-airfoil mechanism of interaction. For values of vertical miss distance larger than h = - 0.01m, the interactions are less and less severe and likewise the separation, resulting in a decrease in magnitude of the negative peaks of drag coefficient associated with reverse flow. However, there are still fluctuations of drag coefficient at the instant when the residual component of the vortex leaves the airfoil, t = 0.0035s. Similar to the case of angle of attack $\alpha = 0^o$, as the residual component of the vortex leaves the airfoil, the drag coefficient converges to a constant value $C_d$ = 0.0073; value which corresponds to the case of a uniform flow past a NACA 0012 airfoil at angle of attack $\alpha = 5^o$, for a Reynolds number 1.3 x $10^6$. From Figure 11 it can be seen that there are differences in the trend of drag coefficient at the instants when the residual component of the vortex is in the near field downstream the airfoil. Hence for vertical miss distances h = 0.00m and h = - 0.005m, the drag coefficient converges to a constant value by an asymptotic growth, while for vertical miss distances h = - 0.01m, h = - 0.015m and h = - 0.02m, the drag coefficient converges to a constant value by an asymptotic decay.

Figure 12 presents the LES results of instantaneous magnitude of velocities for an angle of attack $\alpha = 10^o$, at five different instants in time as a clockwise rotating vortex travels at three different vertical miss-distances, h = 0.00 m, h = - 0.01 m and h = - 0.02m. Similar to the test cases $\alpha = 0^o$ and $\alpha = 5^o$, for an angle of attack $\alpha = 10^o$ the airfoil also sees an induced velocity from the vortex, pointed downward. From Figure 12 it can be seen that the vortex-airfoil mechanism of interaction is a function of both angle of attack and vortex-airfoil vertical miss distance and this is described in the following. From Figure 12 it can be seen that the vortex-airfoil vertical miss distance influences the mechanism of interaction in a particular manner. Hence, for the case of a vertical miss distance h = 0.000m, the vortex-airfoil interaction is severe and the vortex is significantly distorted. The vortex-airfoil mechanism of interaction, for a vertical miss distance h = 0.00m, is associated with distortion of the vortex and

increase of velocity as well large flow separation at the upper surface of airfoil as seen in Figure 12a.

For the test case of a vertical miss distance h = 0.00m, the vortex splits into two residual components, one traveling above the airfoil and the other one traveling underneath the airfoil. The residual component of the vortex, traveling underneath the airfoil exhibits a smaller core size and a weaker strength than the one traveling above the airfoil. As the two residual components of the vortex travel downstream the airfoil, merges into the airfoil wake and disturbs it. As a result of the merging process, the two residual components of the vortex dissipate as they travel far downstream the airfoil.

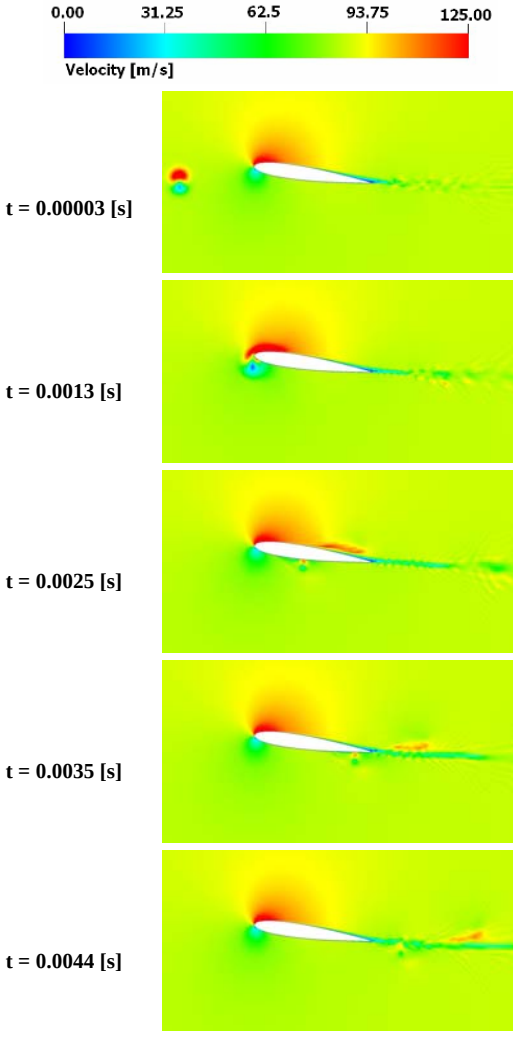


Figure 12. Time evolved fluid structures (velocity magnitude), angle of attack $\alpha = 10^o$

For all test cases, as the residual component of the vortex travels downstream the airfoil and merges with the wake, causes high disturbances of the airfoil wake.

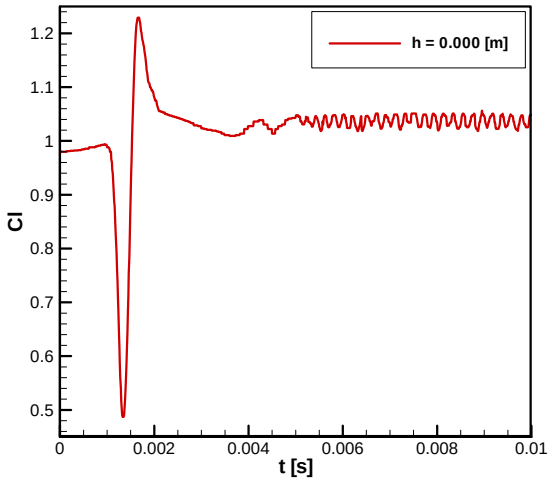


Figure 13. Time history of lift coefficient, $\alpha = 10^o$

The disturbances of the wake are reflected into the fluctuations of the aerodynamic coefficients as seen in Figure 13 and Figure 14 respectively. Figure 13 presents the time varying lift coefficient for the case of an angle of attack $\alpha = 10^o$ and a vortex-airfoil vertical miss distance h = 0.00m. Analog to previous test cases for angles of attack $\alpha = 0^o$ and $\alpha = 5^o$, the lift coefficient presents a similar behavior for test case $\alpha = 10^o$, as seen in Figure 13. The fluctuations of lift coefficient at the instant when the residual component of the vortex leaves the airfoil, t = 0.0035s are still present for angle of attack $\alpha = 10^o$. The disturbances of the wake are reflected into the fluctuations of lift coefficient as seen in Figure 13, after the instant t = 0.005s.

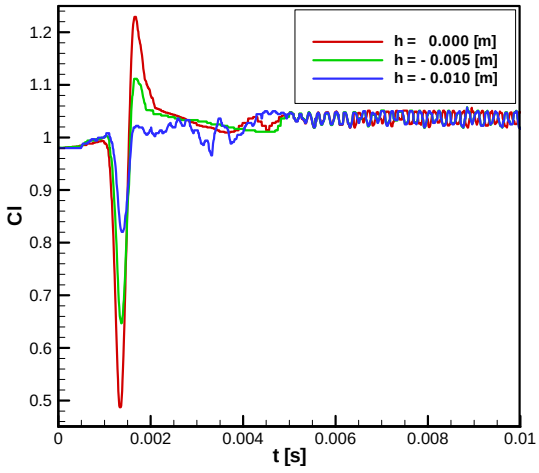


Figure 14. Comparison of lift coefficient, $\alpha = 10^o$

From the comparison of lift coefficient for different vortex-airfoil vertical miss distances, Figure 14, it can be seen that as the vertical miss distance increases, the amplitudes of lift coefficient at the instant when the vortex encounters the airfoil (t = 0.0013s) decrease. As the vortex-airfoil vertical miss distance increases, larger fluctuations of lift coefficient are present as the residual component of the vortex travels the chord length of the airfoil, as seen in Figure 14, for the vertical miss distance h = -0.01m. As the vortex travels far downstream the airfoil, there is a very similar trend in the lift coefficient behavior for all vertical miss distances, as seen in Figure 14, after the instant t = 0.005s.

Figure 15 presents the comparison of lift coefficient for three angles of attack, $\alpha = 0^o$, $\alpha = 5^o$ and $\alpha = 10^o$ respectively, for a vortex-airfoil vertical miss distance h = 0.00m. From Figure 15, it can be seen that with the increase of angle of attack, the amplitude of the lift jump at the instant when the vortex encounters the airfoil, t = 0.0013s, decreases.

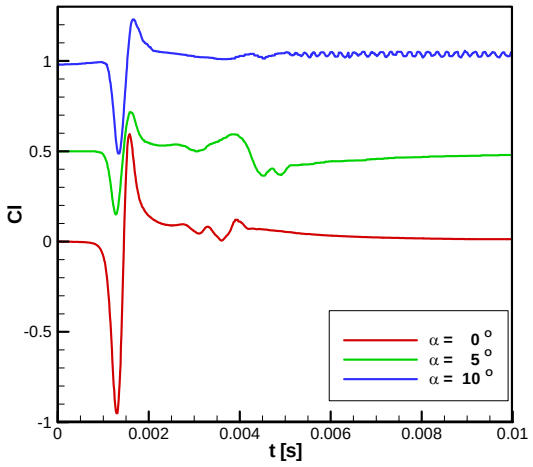


Figure 15. Comparison of lift coefficient, h = 0.000 [m]

Although there are certain similarities in lift coefficient behavior for the three angles of attack, $\alpha = 0^o$, $\alpha = 5^o$ and $\alpha = 10^o$ at the instant when the vortex encounters the airfoil, t = 0.0013s, there are still significant differences between the three test cases at the instant when the residual component of the vortex leaves the airfoil, t = 0.0035s.

Large fluctuations of lift coefficient can be seen for an angle of attack $\alpha = 5^o$, at the instant when the residual component of the vortex leaves the airfoil, and these fluctuations are due to the influence of angle of attack on the vortex-airfoil mechanism of interaction. Also for the angles of attack $\alpha = 0^o$ and $\alpha = 5^o$, there is a difference in lift coefficient behavior, as the vortex leaves the airfoil. Hence for an angle of attack $\alpha = 0^o$, the lift coefficient converges to a constant value by an asymptotic decay, while for an angle of attack $\alpha = 5^o$, the lift coefficient converges to a constant value by an asymptotic growth. For an angle of attack $\alpha = 10^o$, the fluctuations of lift coefficient at the instant when the residual component of the vortex leaves the airfoil are less significant, Figure 15, t = 0.0035s.

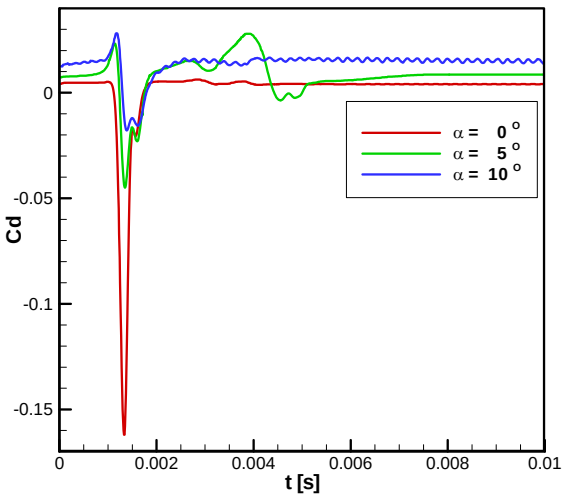


Figure 16. Comparison of drag coefficient, h = 0.000 [m]

Figure 16 presents the comparison of the time varying drag coefficient, for three different angles of attack, for a vortex-airfoil vertical miss distance h = 0.00m. For all three angles of attack $\alpha = 0^o$, $\alpha = 5^o$ and $\alpha = 10^o$ respectively, the vortex-airfoil mechanism of interaction at the instant when the vortex encounters the airfoil, t = 0.0013s, is associated with the flow separation and reverse flow indicated by the large negative values of drag coefficient, Figure 16, at the instant t = 0.0013s. From Figure 16, instant t = 0.0013s, it can be seen that with the increase of angle of attack, the amplitudes of drag coefficient, at the instant when the vortex encounters the airfoil, decrease. Also it can be seen that with the increase of angle of attack, the amount of reverse flow decreases and this is a consequence of the effect of angle of attack on the vortex-airfoil mechanism of interaction. An increase of drag coefficient followed by a sudden decrease can be seen for angles of attack $\alpha = 5^o$ and $\alpha = 10^o$, as the vortex approaches the airfoil. Similar to lift coefficient, large fluctuations of drag coefficient can be seen for an angle of attack $\alpha = 5^o$, at the instant when the residual component

of the vortex leaves the airfoil, t = 0.0035s. These are also consequences of the influence of angle of attack on the vortex-airfoil mechanism of interaction.

## Conclusions

Parametric investigations based on the airfoil angle of attack and vortex-airfoil vertical miss distance were conducted to investigate their influence on the unsteady pressure field about a NACA 0012 airfoil, for a Reynolds number Re = $1.3 \times 10^6$, using LES. The vortex was released upstream of airfoil and the unsteady flow field results were stored at regular time intervals, corresponding to different vortex core locations, along the vortex trajectory and were used for the calculation of the aerodynamic coefficients.

Calculations were made for three different BVI problems based on the airfoil angle of attack, $\alpha = 0^o$, $\alpha = 5^o$ and $\alpha = 10^o$ respectively, with varying the vortex-airfoil offset distance. The presence of the vortex in the flow field induces a velocity at the surface of airfoil, generating a time-varying lift and drag coefficient. The variation of the aerodynamic coefficients depends on the vortex-airfoil mechanism of interaction, defined by airfoil angle of attack and vortex-airfoil vertical miss-distance. For small vertical miss distance values, the vortex–airfoil mechanism of interaction is associated with flow separation and reverse flow.

## References


[1]Hu, H., Jordan,L., CFD Investigation of Double Swept Blade in BVI Noise Reduction, 9th AIAA/CEAS Aeroacoustics Conference, 12-14 May 2003,Hilton Head, SC

[2]Yu, Y., Miss Distance for Blade-Vortex Interaction Noise Reduction, A96-30850

[3]Abello, J., George, A., Wake Displacement Study of Attitude and Flight Parameter Modifications to Reduce Rotorcraft Blade-Vortex Interaction (BVI) Noise, AIAA 2003-3174, 9th AIAA/CEAS Aeroacoustics Conference, 12-14 May 2003,Hilton Head, SC

[4]Chen, J., Chang, D., Unsteady Pressure Measurement for Parallel Vortex-Airfoil Interaction at Low Speed,
Journal of Aircraft Vol.34, No.3, 1997

[5]Felten, F., Lund,T., Numerical Simulation of parallel Airfoil/Vortex Interaction Using a Zonal Hybrid RANS/LES Method, AIAA2005-5127

[6]Nagarajan, S., Lele, S., Prediction of Sound Generated by a Pitching Airfoil: A comparison of RANS and LES, 12th AIAA/CEAS Aeroacoustics Conference, 8-10 May 2006, Cambridge, MA

[7]Wang, M., Moin, P., Computation of Trailing-Edge Flow and Noise Using Large-Eddy Simulation, AIAA Journal, Vol.38, No.12, 2000

[8]Magagnato, E., Sorguven, E., Gabi, M., Far Field Prediction by Large Eddy Simulation and Ffowcs - Willimas Hawkings Analogy, AIAA Paper 3206-2003, May 2003

[9]Bernandini,G., Serafini,J., Gennaretti, M., Aeroelsatic Modeling Effect in Rotor BVI Noise Prediction, 12th AIAA/CEAS Aeroacoustics Conference, 8-10 May 2006, Cambridge, MA

[10]Becker, S., Kaltenbacher, M., Ali, I., Escobar, M., Hahn, C., Sound Generation by Flow around Simple Geometries: Simulation and Experiment, 12th AIAA/CEAS Aeroacoustics Conference, 8-10 May 2006, Cambridge,

[11]Hu, G., and Grossman, B., The Computation of Massively Separated Flows Using Compressible Vorticity Confinement Methods, AIAA Paper 2002-0136,Jan.2002

[12]Oh, W., S., Kim, J.S., Kwon, O.J., Numerical Simulation of Two-Dimensional Blade-Vortex Interactions Using Unstructured Adaptive Meshes, AIAA Journal, Vol. 40., No.3, 2002, pp. 474-480

[13]Lee,S., Reduction of Blade-Vortex Interaction Noise Through Porous Leading Edge, AIAA Journal, Vol.32, No.3, 1994, pp.480-488

[14]Smagorrinsky, J.S., General circulation experiments with the primitive equation, Monthly Weather Rev.91:99-164, 1963

[15]Lilly, D.K., On the application on the eddy viscosity concept in the inertial sub-range of turbulence, NCAR Manuscript, pp195-200, 1996

[16]M. Germano, U. Piomelli, P. Moin, and W. H. Cabot, A dynamic subgrid-scale eddy viscosity model. Phys. Fluids A, 3(7):1760–1765, 1991